J Solid State Electrochem (2009) 13:1351–1359
DOI 10.1007/s10008-008-0682-4

ORIGINAL PAPER

Electrochemical impedance spectroscopic studies of copper dissolution in arginine–hydrogen peroxide solutions

Y. Nagendra Prasad · V. Vinod Kumar · S. Ramanathan

Received: 11 April 2008 / Revised: 9 August 2008 / Accepted: 12 September 2008 / Published online: 9 October 2008

Abstract Anodic dissolution of copper in arginine and hydrogen peroxide-based medium suitable for chemical mechanical planarization slurry formulation was investigated using electrochemical impedance spectroscopy. Potentiodynamic polarization and impedance data were acquired for copper dissolving in hydrogen peroxide and arginine solution. Reaction mechanism analysis (RMA) was employed to determine the mechanistic pathway of copper dissolution. RMA analysis indicates that a stable passivating film does not form on the copper surface, and the direct dissolution of copper was also ruled out. A two-step mechanism involving cupric oxide as an intermediate species is proposed. The data were also fit to an electrical equivalent circuit to obtain insight into the variation of the parameters with the overpotential. The modeled data for the two-step mechanism captures the essential features of the impedance spectra at various overpotentials.

Keywords Anodic dissolution · Electrochemical impedance spectroscopy · Reaction mechanism analysis · Chemical mechanical planarization · Copper · Amino acid

Symbol List

Cu^{+}_{ads}	Charged species of copper adsorbed onto the electrode surface
Cu^{2+}	Charged species of copper in solution
I_{corr}	Corrosion current
R_{sol}	Solution resistance
R_1	Resistance representing non-Faradaic reaction
C_1	Capacitance representing non-Faradaic reaction
R_2	Resistance representing Faradaic reaction
Q	Constant phase element (CPE) representing the double layer
Y_o	Parameter for CPE
n	Exponent for CPE
F	Faraday constant
J	Current (A)
k_{10}, k_{20}	Pre-exponential factors for rate constant
b_1,b_2	Exponents for rate constant
k_1, k_2	Rate constants
V	Overpotential
$Z_{F,m/s}$	Faradaic impedance at metal–solution interface
ω	Frequency
j	imaginary number (square root of −1)
Z_{Total}	Total impedance
θ	Surface coverage of adsorbed species
θ_{ss}	Surface coverage of adsorbed species under steady-state conditions
τ	Total number of surface sites for the given electrode
R_t	Resistance to charge transfer
$Z_{Re_{experimental}}$	Real component of experimentally measured impedance
$Z_{Im_{experimental}}$	Imaginary component of experimentally measured impedance
$Z_{Re_{best\ fit}}$	Real component of best fit impedance
$Z_{Im_{best\ fit}}$	Imaginary component of best fit impedance
w_{Re}	Weight function for the error in real component
w_{Im}	Weight function for the error in imaginary component

Y. Nagendra Prasad · V. Vinod Kumar · S. Ramanathan (✉)
Department of Chemical Engineering,
Indian Institute of Technology-Madras,
Chennai 600036, India
e-mail: srinivar@iitm.ac.in

Introduction

Chemical mechanical planarization (CMP) is a key process used in the formation of copper interconnects in semiconductor

industry [1–3]. CMP involves removal of excess copper using a slurry which consists of chemicals and abrasive particles. In this process, the surface to be planarized is moved against a pad with the slurry flowing between the surface and the pad. The chemicals may etch or modify the surface, while the abrasives would remove the surface by mechanical action. Although acidic slurries are widely used for copper CMP, they tend to corrode the equipment [4]. Recently, an alkaline slurry containing an amino acid L-arginine and hydrogen peroxide was proposed for copper CMP [5]. Arginine has the useful property of suppressing the silicon dioxide polish rate, even at alkaline pH [6].

Copper corrosion in acidic media has been investigated extensively, and the kinetics of dissolution has been analyzed in a wide range of pH and overpotential [7–12]. The dissolution, as well as the deposition, is explained by the two-step mechanism involving an adsorbed intermediate as

$$\begin{aligned} &Cu \rightleftarrows Cu^{+}_{ads} + e^{-} \\ &Cu^{+}_{ads} \rightarrow Cu^{2+} + e^{-} \end{aligned} \quad (1)$$

for low overpotentials. At higher overpotentials, based on the impedance analysis, the following additional steps involving an autocatalytic mechanism have been proposed.

$$\begin{aligned} &Cu^{+}_{ads} \rightleftarrows Cu^{2+}_{ads} + e^{-} \\ &Cu^{2+}_{ads} + Cu \rightarrow Cu^{2+} + Cu^{2+}_{ads} + 2\,e^{-} \end{aligned} \quad (2)$$

In the acidic pH range, particularly at low overpotentials, cuprous and cupric oxides are not expected to be present [13]. Hence, the models proposed for copper dissolution in acidic medium do not include any film on the metal surface. In alkaline medium, passivating films are formed on the copper surface. The nature of the film and the kinetics of film formation have been investigated by electrochemical and non-electrochemical techniques [14–26], and it was shown that a typical film consists of Cu_2O, CuO, and $Cu(OH)_2$ layers [15, 21, 23]. However, most of the studies have focused on the film formation in alkaline solutions which do not contain any additional oxidizing or complexing agent. Arginine is an effective complexing agent which can remove the copper oxide layers. Although arginine and hydrogen peroxide have been shown to be a suitable combination for Cu CMP slurry, the mechanism of the dissolution of copper in this medium is not understood well [5]. There are limited reports on the kinetics of copper dissolution in an alkaline solution containing a complexing agent and hydrogen peroxide [5, 27]. In this work, we probe the copper dissolution using potentiodynamic polarization and electrochemical impedance spectroscopy (EIS). Reaction mechanism analysis (RMA) and electrical equivalent circuit (EEC) are employed to model the system. From a detailed comparison of the model predictions and the experimental data, we propose a two-step reaction mechanism involving an oxide intermediate species.

Experimental

A standard three-electrode cell, with an Ag/AgCl (3.5 M KCl) reference electrode, a platinum counter electrode (both from CH Instruments), and a copper rod of 11 mm diameter (99.9999%+ purity, Sigma-Aldrich) as the working electrode, was used. All the potentials reported are with respect to the Ag/AgCl electrode. MilliQ water (Millipore) was used in preparing the solutions, and all the chemicals used were of AR grade. The working electrode was polished with successively finer powders of alumina (Buehler) and ultrasonicated immediately before each experiment. The following solution compositions was employed. One percent (vol/vol) hydrogen peroxide, 1% (wt) arginine, and 0.1 M sodium sulfate as supporting electrolyte. Potentiodynamic polarization experiments were also conducted in solutions without arginine. For the experiments without arginine, the pH was adjusted to 10 using concentrated sodium hydroxide. All the experiments were conducted at room temperature, and the solutions did not contain any abrasive powder.

The potentiodynamic and impedance data were acquired with PARSTAT 2263 (EG&G Princeton Applied Research). Potentiodynamic polarization curves were obtained by sweeping the voltage from cathodic to anodic potential at 2 mV s^{-1}. The impedance data were obtained by applying an ac perturbation of 20 mV (peak to peak) in the frequency range of 50 mHz to 50 kHz at various DC potentials where dissolution occurs. Zsimpwin software was used to determine the EEC parameters by complex non-linear least square (CNLS) analysis. The RMA parameters were estimated using sequential quadratic programming.

Results and discussion

Potentiodyanmic polarization measurements

The potentiodynamic polarization plots for copper in 1% (vol/vol) hydrogen peroxide and 0.1 M sodium sulfate with and without L-arginine are shown in Fig. 1. For the system with only hydrogen peroxide, the anodic current branch is lower, indicating the possible formation of a film. Copper in alkaline media will tend to form cuprous and cupric oxides and copper hydroxide film [13–26]. The film may not completely passivate the surface but may still decrease the dissolution rate [28]. Figure 1 shows that, in the presence of arginine, the anodic branch does not exhibit any sign of passivation. The anodic and cathodic branches were

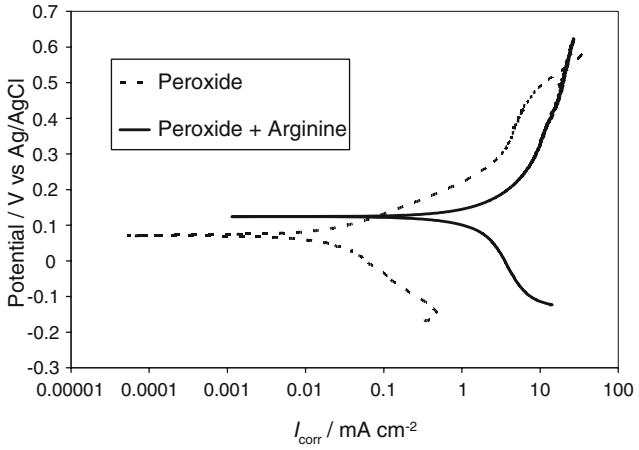

Fig. 1 Potentiodynamic polarization curves for copper in solution containing 1% (vol/vol) hydrogen peroxide and 0.1 M sodium sulfate with and without 1% (wt) arginine, at a pH of 10

extrapolated, and the corrosion current (I_{corr}) was estimated using the software PowerCorr. It was found that the corrosion currents were 4,000 and 17 μA cm^{-2} for the system with and without arginine, respectively. The large increase in I_{corr} with the addition of arginine shows that the dissolution rate of copper increases significantly in the presence of arginine and hydrogen peroxide. Potential pH diagram for a simple amino acid glycine reveals that the addition of glycine reduces the stability region of CuO, and copper–glycine complex formation is preferred [29]. It is quite likely that arginine also reduces the stability region of CuO and would tend to complex the cupric ions and thus dissolve the film. This would explain the lack of any sign of passivation in the anodic branch of the polarization curve for copper dissolution in arginine and hydrogen peroxide. However, the possibility of copper oxide or copper hydroxide formation at alkaline pH, at least as an intermediate species, exists [13–26]. Hence, it can be concluded that direct dissolution of copper is not likely to occur in this system and that a thick, stable passivating oxide is also not likely to be present.

EIS measurements

EIS is a powerful tool that can be used to unravel the mechanism of electrochemical reactions [30–35]. The kinetics of dissolution and passivation of various metals in acidic media have been successfully analyzed with EIS [36–39]. Experimental EIS data for copper electrode in 1% (vol/vol) hydrogen peroxide and 1% (wt) arginine with 0.1 M sodium sulfate as the supporting electrolyte at various overpotentials are shown as data points in the Nyquist representation in Fig. 2. The overpotentials were chosen based on the results of potentiodynamic polarization curves (Fig. 1). The open circuit potential (OCP) of the copper electrode in arginine–hydrogen peroxide system was 140 mV vs Ag/AgCl, and hence the EIS data were acquired at anodic potentials with an interval of 50 mV starting at the OCP. In the high frequency regime, a capacitive loop corresponding to the double layer regime is observed, while in the low frequency regime, an additional capacitive loop corresponding to the dissolution reaction is observed. The loop at high frequencies shrinks with the overpotential, while the loop at low frequencies expands. In the low frequency loop, a linear region at 45° from the real axis can be observed, particularly at the potential of 290 mV vs Ag/AgCl. Usually, a 45° line in the Nyquist plot is associated with diffusion-limited regime, and the implications are discussed later.

Reaction mechanism analysis

The equations of impedance for various reaction mechanisms have been reported [40–44] and are summarized here for the candidate mechanisms. The following assumptions are employed in the derivation of the impedance equations: (1) The adsorption of the intermediate species follows Langmuir isotherm model; (2) The rate constants depend on the potential exponentially, similar to Tafel parameters; and (3) The ac perturbation is small so that the nonlinear terms can be neglected. When the amplitude of the exiting signal is 10 mV or less, the system response would tend to be linear [45]. It is to be noted that the linearity of a system depends on several factors including the electrode surface, electrochemical cell configuration, etc. Since the data show a depressed semicircle, especially at higher frequency, a constant phase element (CPE), rather than a simple capacitor, was employed to represent the double layer. A CPE is represented by the parameters Y_o and n and may be observed when the electrode surface is not uniform [46,

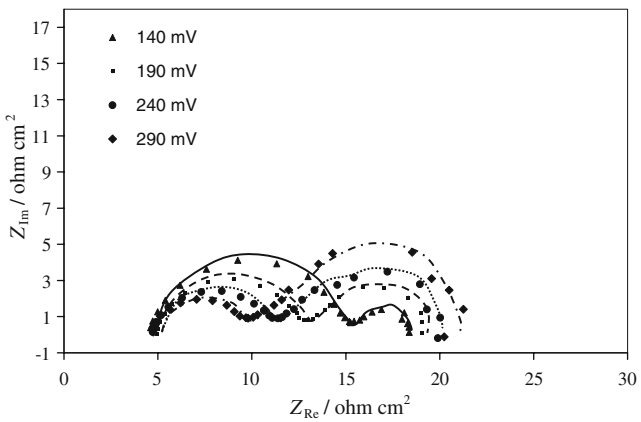

Fig. 2 Experimental EIS data at various overpotentials for copper in 1% (vol/vol) hydrogen peroxide, 1% (wt) arginine, and 0.1 M sodium sulfate. The *lines* are drawn for guiding the eye and they do not represent any data fit

47]. While the exact source of the CPE behavior is not agreed upon yet, it is widely used to represent the double layer which exhibits frequency dispersion of capacitance [48–52].

Inapplicability of the direction dissolution reaction

Consider the simple direct dissolution reaction given in Eq. 3. The current (J) and the rate constants are given in Eq. 4 where F is the Faraday constant and V is the overpotential.

$$\mathrm{Cu} \xrightarrow{k_1} \mathrm{Cu}^{2+} + 2e^- \tag{3}$$

$$\begin{aligned} J &= Fk_1 \\ k_1 &= k_{10} e^{b_1 V} \end{aligned} \tag{4}$$

Here k_1 is the rate constant, k_{10} is the pre-exponential factor, and b_1 is the exponent which represents the potential barrier in the direction of the reaction. The Faradaic impedance at the metal–solution interface $Z_{\mathrm{F,m/s}}$ and the total impedance of the system Z_{Total} are given respectively by

$$\frac{1}{Z_{\mathrm{F,m/s}}} = \frac{dJ}{dV} = Fk_1 b_1 = Fk_{10} b_1 e^{b_1 V} \tag{5}$$

$$Z_{\mathrm{Total}} = R_{\mathrm{sol}} + \left(\left(Z_{\mathrm{F,m/s}} \right)^{-1} + (j\omega)^n Y_o \right)^{-1} \tag{6}$$

Here R_{sol} is the solution resistance and ω is the angular frequency of the applied ac voltage. Equation 5 shows that the Faradaic impedance decreases with an increase in overpotential and that it is independent of frequency of perturbation for this mechanism. Thus, it is clear that the impedance modeled by the direct dissolution mechanism can give rise to only one capacitance loop which corresponds to the CPE as given in Eq. 6. Hence, the mechanism given by Eq. 3 cannot represent the dissolution of copper in the arginine and peroxide solution. A reaction involving at least one intermediate species is necessary to adequately model this system.

Proposed reaction mechanism

The dissolution of copper in glycine and hydrogen peroxide system at pH 4 has been investigated with Fourier transformed EIS, and the role of hydrogen peroxide and the amino acid has been delineated [53]. Normally, hydrogen peroxide would react with copper to form cuprous and cupric oxides. However, in the presence of Cu–amino acid complexes, hydrogen peroxide dissociates into hydroxyl radicals (*OH) which are powerful oxidizing agents [54]. For glycine and hydrogen peroxide-based solutions, hydroxyl radicals would convert the copper to copper oxide by the reaction

$$\mathrm{Cu} + 2\,(^*\mathrm{OH}) \rightarrow \mathrm{CuO} + \mathrm{H_2O}. \tag{7}$$

The oxide would subsequently be dissolved by the complexing action of amino acid [48]. It was also proposed that the direct dissolution transfer ($\mathrm{Cu} \rightarrow \mathrm{Cu}^{2+}_{\mathrm{sol}} + 2e^-$) was unlikely in the presence of hydrogen peroxide [53]. It is likely that arginine and peroxide, in the presence of copper, also produce significant amounts of hydroxyl radicals which oxidize the copper surface. Hence, a candidate mechanism involving one intermediate species and two more parameters k_{20} and b_2 was chosen. The reaction between the hydroxyl radical and the copper surface can be described by the Faradaic reaction given below.

$$\mathrm{Cu} + (^*\mathrm{OH}) \xrightarrow{k_1} \mathrm{CuO} + \mathrm{H}^+ + e^- \tag{8}$$

This may proceed in parallel with the reaction given by Eq. 7. In alkaline pH, the product H^+ ion in Eq. 8 would react with hydroxyl ions to form water, and the cupric oxide would be dissolved by arginine through non-Faradaic reactions similar to the dissolution of copper oxide by glycine. At a pH value of 10, arginine would be present mostly as neutral species, as given in Fig. 3 [55]. It may complex with CuO and may dissolve as given in Eq. 9 where HX is the form given in Fig. 3. The non-Faradaic reactions are similar to the dissolution of copper by glycine [48].

$$\mathrm{CuO} + 2\mathrm{HX} \xrightarrow{k_2} \mathrm{Cu[X]_2} + \mathrm{H_2O} \tag{9}$$

Cuprous and cupric oxides and cupric hydroxides are expected to be present on the copper surface at alkaline pH [7, 14–26]. However, in the presence of complexing agents such as ammonia which dissolve the oxide, they may not completely cover the surface but rather be present at submonolayer coverage [13]. Thus, it is unlikely that copper surface in arginine and peroxide solution is completely covered by a thick film of oxide. The potentiodynamic polarization data (Fig. 1) also does not show any evidence for the presence of a passivating oxide film. Hence, the impedance caused by a possible thick oxide film is not considered in this analysis.

For the reaction given by Eqs. 8 and 9, with the intermediate species CuO having a surface coverage θ, the unsteady-state mass balance can be written as

$$\tau \frac{d\theta}{dt} = k_1 (1 - \theta) - k_2 \theta \tag{10}$$

where τ is the total number of surface sites per unit area for the given electrode surface. Under steady-state conditions,

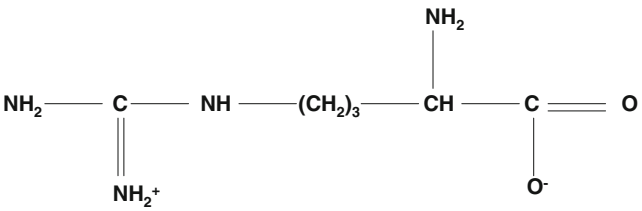

Fig. 3 The structure of L-arginine at pH of 10

the surface coverage (θ_{ss}) and the current due to Faradaic reaction (J) respectively are given below:

$$\theta_{SS} = \frac{k_1}{k_1 + k_2}. \tag{11}$$

$$J = F\, k_1 (1 - \theta) \tag{12}$$

The Faradaic impedance ($Z_{F,m/s}$) is obtained by taking the derivative of the current given in Eq. 12 with respect to the voltage, and it is given by

$$\begin{aligned} \frac{dJ}{dV} &= \left(Z_{F,m/s}\right)^{-1} = F \frac{d}{dV}\left(k_{10}\, e^{b_1 v}(1-\theta)\right) \\ &= F\, k_{10}\, e^{b_1 v}\left(b_1(1-\theta_{SS}) - \frac{d\theta}{dV}\right) \end{aligned} \tag{13}$$

However, from Eq. 11, $k_1(1-\theta_{SS}) = k_2\theta_{SS}$. By expanding the Eq. 10 in series form and neglecting the second- and higher-order terms, it is seen that

$$\begin{aligned} \tau \frac{d\theta}{dV}\frac{dV}{dt} &= (k_1 + b_1 k_1 V)\left(1 - \theta_{SS} - \frac{d\theta}{dV}\right) - (k_2 + b_2 k_2 V)\left(\theta_{SS} + \frac{d\theta}{dV}\right) \\ j\omega\tau \frac{d\theta}{dV} &= (k_1 + k_2)\left(-\frac{d\theta}{dV}\right) + b_1 k_1 (1 - \theta_{SS}) - b_2 k_2 \theta_{SS} \end{aligned} \tag{14}$$

Thus

$$\begin{aligned} \left(Z_{F,m/s}\right)^{-1} &= (R_t)^{-1} - F\, k_1 \frac{d\theta}{dV}, \text{where} \\ (R_t)^{-1} &= F\, b_1\, k_2\, \theta_{SS} \\ \frac{d\theta}{dV} &= \frac{(b_1 - b_2) k_2 \theta_{SS}}{k_1 + k_2 + j\omega\tau} \end{aligned} \tag{15}$$

Here, R_t represents the resistance to charge transfer. It is seen from Eq. 15 that, when the parameter b_1 is greater than b_2, the rate of change of surface coverage with potential is positive. In this case, Faradaic impedance will decrease with the frequency, and the impedance behavior will resemble that of a capacitor. The total impedance (Z_{Total}) is given by the equation

$$Z_{Total} = R_{sol} + \frac{1}{Y_0 (j\omega)^n + \left(Z_{F,m/s}\right)^{-1}} \tag{16}$$

The best fit spectra are shown in Fig. 4 as dotted lines along with the experimental data points. The corresponding parameters are shown in Table 1. The solid lines in Fig. 4 are best fit results for the EEC discussed later. It is to be noted that except for the parameters Y_o and n, the values in the table are applicable for all the voltages. The actual rate constants k_1 and k_2 at each overpotential can be calculated using the formula given in Eq. 4. The parameter set for the mechanism was obtained by sequential quadratic programming method, minimizing the error term given by

$$\text{error} = \sum \left[w_{Re}\left(Z_{Re_{experimental}} - Z_{Re_{best\ fit}}\right)^2 + w_{Im}\left(Z_{Im_{experimental}} - Z_{Im_{best\ fit}}\right)^2 \right] \tag{17}$$

taken over all the frequencies and voltages. Here, w_{Re} and w_{Im} are the weighing functions which could be chosen as unity or as the inverse of the square of the real and imaginary part of the experimental impedance. The errors in the impedance measurements can be heteroskedastic, i.e., a strong function of frequency. Specifically, if the impedance values span over an order of magnitude or more, the choice of weight function would make a significant difference in the values of the optimized parameter set, and the unity weight function may not be the appropriate choice. However, in this case, all the impedance values were between 5 and 25 Ω in magnitude, and the fitted parameters were not sensitive to the weight function chosen. The values listed in Table 1 are based on the unity weight function.

EEC model of the Cu–solution interface

Harrington and van den Driessche have shown that, for a particular class of reaction mechanisms, the equivalent circuits can be made with resistors and capacitors alone [34]. EIS data could be modeled either by assuming an electrical circuit and obtaining the parameter by regression or by sequential regression of the line shapes to the data [56]. For example, a series of elements in Voight circuit can be used to fit data simulated by circuits containing capacitors, inductors, Warburg impedance, or CPE. The number of time constants captured in the data could be determined by the number of Voight elements necessary to obtain a low residual sum of squares. When adding more Voight elements does not result in a significant reduction in the residual sum of squares, the fit would be considered adequate to describe the data. Since the EIS data in Fig. 2 show two loops which may be described by two capacitors, the method of sequential regression was not chosen, and instead the data was fit to the equivalent circuit shown in Fig. 5. In Fig. 5, R_{sol} is the solution resistance and Q represents the CPE. R_2 represents the resistance to Faradaic reactions while R_1 and C_1 can be interpreted as the resistance and capacitance associated with the non-Faradaic reaction. In the literature, a slightly more complicated circuit has been employed to describe the Fourier transform-electrochemical impedance spectra of dissolution of copper in glycine and hydrogen peroxide [53].

It is seen that the basic characteristics of the experimental data are captured well by the EEC. All the estimated

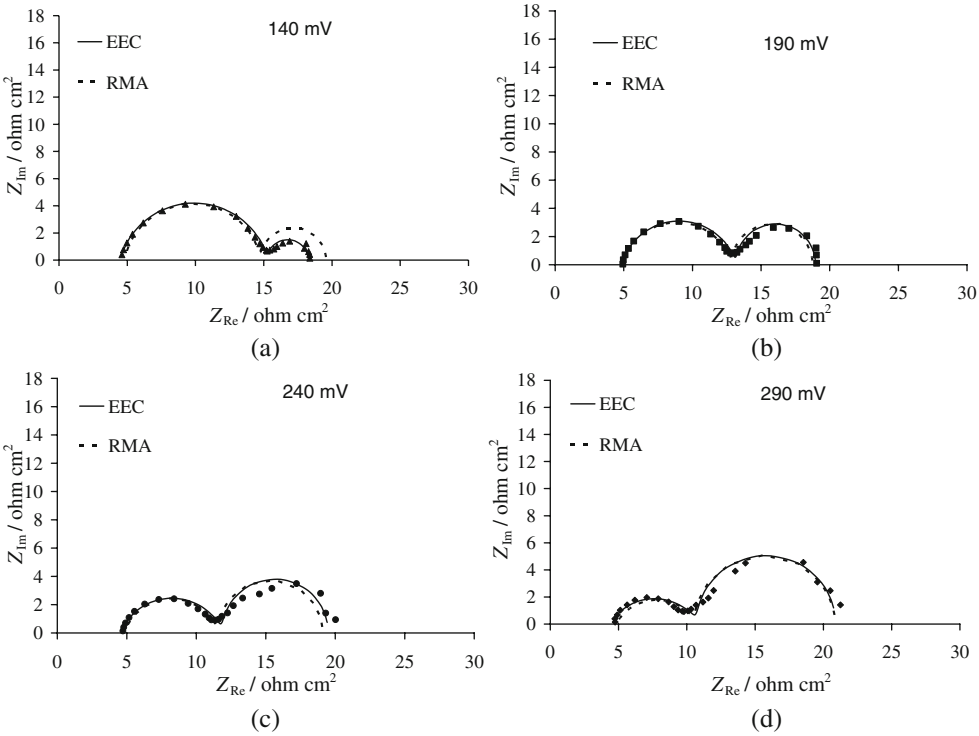

Fig. 4 Best fit EIS values superimposed with experimental data at **a** 140 mV, **b** 190 mV, **c** 240 mV, and **d** 290 mV (vs Ag/AgCl) for copper in 1% (vol/vol) hydrogen peroxide, 1% (wt) arginine, and 0.1 M sodium sulfate. Both electrical equivalent circuit (*EEC*) best fit results and the reaction mechanism analysis (*RMA*) best fit results are shown

parameters except R_{sol} are plotted against the overpotential in Fig. 6. The solution resistance is estimated to be about 4.79± 0.28 Ω for all the four spectra. From Fig. 6b, it is seen that R_2 decreases slightly with increase in the overpotential, indicating that the Faradaic reaction may be enhanced at higher potentials. With an increase in overpotential, R_1 increases while C_1 decreases as seen from Fig. 6a. Since R_1 and C_1 are associated with the same reaction, they are expected to be coupled and show trends in mutually opposite directions [53]. While the increase in R_1 with overpotential may be partly compensated by the decrease in R_2, the decrease in C_1 with overpotential would result in an increase in impedance as seen in the low frequency loop of Fig. 2. Since the dissolution rate of the copper in arginine and hydrogen peroxide solution is high, the total impedance is low. It is seen that at the high frequency limits the total impedance can be approximated by the estimated solution resistance and at the low frequency limits the impedance can be approximated by the sum of the three resistances in the circuit given in Fig. 5. The parameter values associated with CPE are shown in Fig. 6c. The Y_o and n values estimated by EEC (shown in Fig. 6c) are very similar to the estimates obtained for RMA, shown in Table 1. It is clear that the exponent n deviates from the ideal value of 1 as the overpotential increases. At the low overpotential of 140 mV vs Ag/AgCl, the parameter is about 0.85. However, at the higher overpotential of 290 mV vs Ag/AgCl, the value for n is about 0.65. The parameter value of 0.85 would indicate

Table 1 Parameters used for the RMA

Parameter		Value	Units
k_{10}		1.58×10^{-7}	moles cm^{-2} s^{-1}
b_1		6.60	V^{-1}
k_{20}		5.84×10^{-7}	moles cm^{-2} s^{-1}
b_2		−0.97	V^{-1}
τ		7.43×10^{-8}	moles cm^{-2}
Y_o at various DC potentials	OCP	3.86×10^{-5}	Ω^{-1} cm^{-2} s^n
	OCP+50 mV	7.92×10^{-5}	
	OCP+100 mV	1.26×10^{-4}	
	OCP+200 mV	3.68×10^{-4}	
n at various DC potentials	OCP	0.90	–
	OCP+50 mV	0.82	
	OCP+100 mV	0.79	
	OCP+200 mV	0.69	
R_{sol}		4.81	Ω cm^2

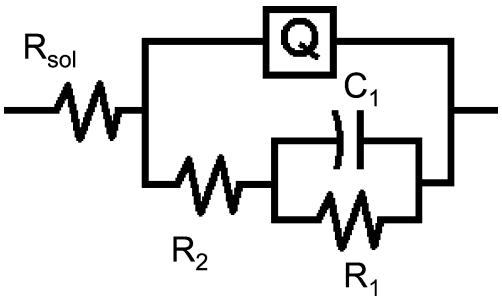

Fig. 5 Electrical equivalent circuit for copper in 1% (vol/vol) hydrogen peroxide, 1% (wt) arginine, and 0.1 M sodium sulfate

that the electrode surface has a significant roughness at OCP. At higher potentials, the dissolution rate and subsequently the surface roughness would increase, resulting in a lower value for n. However, a value as low as 0.65 would indicate that diffusion effects come into play since a value of 0.5 for the exponent n would correspond to Warburg impedance which essentially represents diffusion [46]. This is also seen from the clearer appearance of the 45° line in the low frequency loop, with increasing overpotential. The parameter Y_o is seen to increase with the overpotential. Even for smooth electrodes which exhibit an ideal capacitance behavior, the double layer capacitance value may depend on the voltage [57], perhaps due to the change in specific adsorption of anions. In this case, the best value for n is 0.85 at the OCP, and this would correspond to a significant roughness of the electrode surface. With the electrode exhibiting non-ideal behavior, it is not surprising that both Y_o and n vary with the potential in this case.

A comparison of the other parameters estimated and the trends in the EEC show that the resistance R_2 would correspond to the reaction given in Eq. 8. Since the value of b_1 is positive, an increase in overpotential would increase the corresponding reaction, thereby reducing the resistance. Similarly, the negative value of b_2 and the increase in value of R_1 with the overpotential indicate that the electrical elements R_1 and C_1 are associated with the reaction given in Eq. 9.

The main features of the EIS data are captured well by the RMA. Specifically, with increase in DC overpotential, (1) the capacitance loop in the high frequency regime shrinks, (2) the capacitance loop in the low frequency regime expands, and (3) the point of intersection of the two capacitance loops moves to the right. A specific characteristic that is not captured by RMA is the reduction in the overall impedance at the lowest frequency with increase in overpotential. Particularly, the best fit plot corresponding to 140 mV (vs Ag/AgCl) deviates more from the experimental data compared to the best fit results at higher overpotentials. The difference may be due to possible interference by other reactions near OCP that are not considered in the mechanistic analysis. The order of magnitude of the parameters estimated compare well with those reported in literature for other metal dissolution reactions [38–40]. In the overpotential region investigated, both k_1 and k_2 are of comparable value, and hence the overall rate of reaction depends on both parameters. It is to be noted that the reactions given in Eqs. 7, 8, and 9 may be reversible. It is seen that the data can

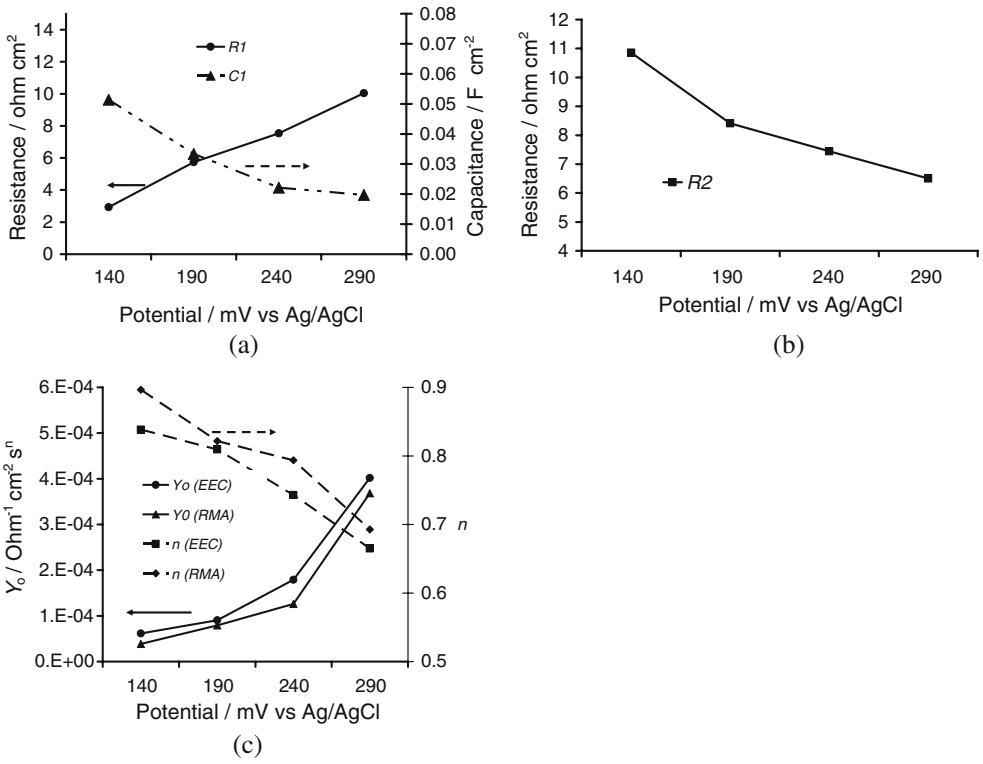

Fig. 6 Parameters of electrical equivalent circuit corresponding to **a** non-Faradaic reaction, **b** Faradaic reaction, and **c** constant phase element for the equivalent circuit shown in Fig. 5 plotted against the DC potential of the electrode

be fitted well with forward reactions alone, which means that the rates of reverse reactions may be low in the concentration and potential ranges investigated. The proposed reactions (Eqs. 8 and 9) indicate that the copper surface is covered with a sub-monolayer of CuO. The existence, composition, and the surface coverage of the film have to be verified by other techniques such as electrochemical scanning tunneling microscopy or spectroscopic techniques. Based on the results, the kinetic model could be modified suitably to explain the impedance as well as other results in a consistent manner and a more thorough understanding of the dissolution mechanism would be possible. The EEC may also need to be modified to account for all the processes occurring in the system.

Conclusions

The dissolution mechanism of copper in arginine and hydrogen peroxide medium was investigated using potentiodynamic polarization and EIS technique. Potentiodynamic data indicate the absence of passivation even at alkaline pH. EIS data show a capacitance loop at high frequencies corresponding to double layer capacitance and an additional capacitance loop at lower frequencies corresponding to non-Faradaic relaxation processes. Electrical equivalent circuit analysis and reaction mechanism analysis were employed to fit the EIS data, and based on the comparison of the experimental and the best fit data, as well as potentiodynamic results, the direct dissolution of copper was ruled out. A two-step mechanism involving a Faradaic reaction between the hydroxyl radicals and the copper surface with cupric oxide as the product [14–26] and the subsequent dissolution of cupric oxide by complexation [53] is proposed. Both EEC analysis and RMA capture the essential features of the experimental results obtained at various overpotentials. Further analysis of the copper surface in arginine and peroxide solution by complementary techniques is necessary to confirm the presence of the intermediate oxide species and to understand their characteristics.

Acknowledgments The authors would like to thank the Ministry of Human Resource Development (MHRD), India for funding this project (CHE/0304/065/MHRD/SRAT).

References

1. Steigerwald JM, Murarka SP, Gutmann RJ (1997) Chemical mechanical planarization of microelectronic materials. Wiley, New York
2. Oliver MR (2004) In: Oliver MR (ed) Chemical–mechanical planarization of semiconductor materials. Springer, Berlin
3. Anik M (2005) J Appl Electrochem 35:1. doi:10.1007/s10800-004-1763-4
4. Luo Q, Campbell DR, Babu SV (1997) Thin Solid Films 311 (1–2):177. doi:10.1016/S0040-6090(97)00454-9
5. Prasad YN, Ramanathan S (2007) Electrochim Acta 52(22):6353. doi:10.1016/j.electacta.2007.04.044
6. Her Y-S, Srinivasan R, Babu SV, Ramarajan S (2006) U.S. Patent 7101800
7. Cordeiro GGO, Barcia OE, Mattos OR (1993) Electrochim Acta 38(2–3):319. doi:10.1016/0013-4686(93)85146-P
8. Turner M, Brook PA (1973) Corros Sci 13:973. doi:10.1016/S0010-938X(73)80080-0
9. Braun M, Nobe K (1979) J Electrochem Soc 126(10):1666. doi:10.1149/1.2128773
10. Brossard L (1983) J Electrochem Soc 130(2):403. doi:10.1149/1.2119719
11. Stankovic ZD (1983) Electrochim Acta 28(1):109. doi:10.1016/0013-4686(83)85092-0
12. Glarum SH, Marshall JH (1985) J Electrochem Soc 132(12):2878. doi:10.1149/1.2113687
13. Pourbaix M (1974) Atlas of electrochemical equilibria in aqueous solutions, 2nd edn. NACE, Houston
14. Strehblow HH, Titze B (1980) Electrochim Acta 25(6):839. doi:10.1016/0013-4686(80)90036-5
15. Sander U, Strehblow HH, Dohrmann JK (1981) J Phys Chem 85 (4):447. doi:10.1021/j150604a025
16. Lohrengel MM, Schultze JW, Speckmann HD, Strehblow HH (1987) Electrochim Acta 32(5):733. doi:10.1016/0013-4686(87)85103-4
17. Gomez Becerra J, Salvarezza RC, Arvia AJ (1988) Electrochim Acta 33(5):613. doi:10.1016/0013-4686(88)80059-8
18. Collisi U, Strehblow HH (1990) J Electroanal Chem 284:385. doi:10.1016/0022-0728(90)85046-8
19. Melendres CA, Bowmaker GA, Leger JM, Beden B (1998) J Electroanal Chem 449:215. doi:10.1016/S0022-0728(97)00609-8
20. Maurice V, Strehblow HH, Marcus P (2000) Surf Sci 458:185. doi:10.1016/S0039-6028(00)00442-8
21. Babic R, Metikos-Hukovic M, Jukic A (2001) J Electrochem Soc 148(4):B146. doi:10.1149/1.1354608
22. Kunze J, Maurice V, Klein LH, Strehblow HH, Marcus P (2003) J Electroanal Chem 554–555:113. doi:10.1016/S0022-0728(03)00115-3
23. Kunze J, Maurice V, Klein LH, Strehblow HH, Marcus P (2004) Corros Sci 46:245. doi:10.1016/S0010-938X(03)00140-9
24. Folquer ME, Ribotta SB, Real SG, Gassa LM (2002) Corr 58 (3):240
25. Nishikata A, Itagaki M, Tsuru T, Haruyama S (1990) Corros Sci 31:287. doi:10.1016/0010-938X(90)90121-K
26. Perez Sanchez M, Barrera M, Gonzalez S, Souto RM, Salvarezza RC, Arvia AJ (1990) Electrochim Acta 35(9):1337. doi:10.1016/0013-4686(90)85004-7
27. Aksu S, Wang L, Doyle FM (2003) J Electrochem Soc 150(11): G718. doi:10.1149/1.1615611
28. Ein-Eli Y, Starosvetsky O (2007) Electrochim Acta 52(5):1825. doi:10.1016/j.electacta.2006.07.039
29. Tamilmani S, Huang W, Raghavan S, Small R (2002) J Electrochem Soc 149:G638. doi:10.1149/1.1516224
30. Keddam M (1995) In: Marcus P, Oudar J (eds) Corrosion mechanism in theory and practice. Marcel Dekker, New York
31. Macdonald DD, McKubre MCH (2005) In: Barsoukov E, Macdonald JR (eds) Impedance spectroscopy. 2nd edn. Wiley, New Jersey
32. Diard J-P, Le Gorrec B, Montella C (1992) J Electroanal Chem 326:13. doi:10.1016/0022-0728(92)80500-4
33. Diard J-P, Le Gorrec B, Montella C (1993) J Electroanal Chem 352:1. doi:10.1016/0022-0728(93)80250-L

34. Harrington DA, van den Driessche P (2004) J Electroanal Chem 567:153. doi:10.1016/j.jelechem.2003.12.020
35. Gregori J, Gimenez-Romero D, Garcia-Jareno JJ, Vicente F (2005) J Solid State Electrochem 9:83. doi:10.1007/s10008-004-0557-2
36. Ashrafi A, Golozar MA, Mallakpour S (2008) J Appl Electrochem 38:225. doi:10.1007/s10800-007-9429-7
37. Assiongbon KA, Emery SB, Gorantla VRK, Babu SV, Roy D (2005) Corros Sci 48(2):272
38. Baril G, Galicia G, Deslouis C, Pebere N, Tribollet B, Vivier V (2007) J Electrochem Soc 154(2):C108. doi:10.1149/1.2401056
39. Gregori J, Garcia-Jareno JJ, Gimenez-Romero D, Roig A, Vicente F (2007) J Electrochem Soc 154(7):C371. doi:10.1149/1.2737665
40. Keddam M, Mattos OR, Takenouti H (1981) J Electrochem Soc 128:257. doi:10.1149/1.2127401
41. Keddam M, Mattos OR, Takenouti H (1981) J Electrochem Soc 128:266. doi:10.1149/1.2127402
42. Macdonald DD, Real S, Smedley SI, Urquidi-Macdonald M (1988) J Electrochem Soc 135:2410. doi:10.1149/1.2095348
43. Bojinov M (1996) J Electroanal Chem 405:15. doi:10.1016/0022-0728(95)04392-6
44. Gregori J, Gimenez-Romero D, Garcia-Jareno JJ, Vicente F (2006) J Solid State Electrochem 10:920. doi:10.1007/s10008-005-0038-2
45. Darowicki K (1995) Corros Sci 37(6):913. doi:10.1016/0010-938X(95)00004-4
46. Rammelt U, Reinhard G (1990) Electrochim Acta 35(6):1045. doi:10.1016/0013-4686(90)90040-7
47. Pajkossy T (2005) Solid State Ion 176:1997. doi:10.1016/j.ssi.2004.06.023
48. Zoltowski P (1998) J Electroanal Chem 443:149. doi:10.1016/S0022-0728(97)00490-7
49. Sadkowski A (2000) J Electroanal Chem 481:222. doi:10.1016/S0022-0728(99)00480-5
50. Lang G, Heusler KE (2000) J Electroanal Chem 481:227. doi:10.1016/S0022-0728(99)00481-7
51. Zoltowski P (2000) J Electroanal Chem 481:230. doi:10.1016/S0022-0728(99)00482-9
52. Sadkowski A (2000) J Electroanal Chem 481:232. doi:10.1016/S0022-0728(99)00483-0
53. Lu J, Garland JE, Pettit CM, Babu SV, Roy D (2004) J Electrochem Soc 151:G717. doi:10.1149/1.1795256
54. Hariharaputhiran M, Zhang J, Ramarajan S, Keleher JJ, Li Y, Babu SV (2000) J Electrochem Soc 147:3820. doi:10.1149/1.1393979
55. Lehinger L (1984) Principles of biochemistry, 2nd edn. CBS, New Delhi
56. Agarwal P, Orazem ME, Garcia-Rubio LH (1992) J Electrochem Soc 139(7):1917. doi:10.1149/1.2069522
57. Srinivasan R, Suni II (1998) J Appl Electrochem 28:993. doi:10.1023/A:1003405329562